

1 **Objects in *Kepler's* Mirror May be Larger Than They Appear:**
2 **Bias and Selection Effects in Transiting Planet Surveys**

3 Eric Gaidos

4 Department of Geology and Geophysics, University of Hawai'i at Mānoa, Honolulu, HI
5 96822

6 gaidos@hawaii.edu

7 and

8 Andrew W. Mann

9 Institute for Astronomy, University of Hawai'i at Mānoa, Honolulu, HI 96822

10 Received _____; accepted _____

Accepted to *The Astrophysical Journal*

ABSTRACT

11

12

Statistical analyses of large surveys for transiting planets such as the *Kepler* mission must account for systematic errors and biases. Transit detection depends not only on the planet’s radius and orbital period, but also on host star properties. Thus, a sample of stars with transiting planets may not accurately represent the target population. Moreover, targets are selected using criteria such as a limiting apparent magnitude. These selection effects, combined with uncertainties in stellar radius, lead to biases in the properties of transiting planets and their host stars. We quantify possible biases in the *Kepler* survey. First, Eddington bias produced by a steep planet radius distribution and uncertainties in stellar radius results in a 15-20% overestimate of planet occurrence. Second, the magnitude limit of the *Kepler* target catalog induces Malmquist bias towards large, more luminous stars and underestimation of the radii of about one third of candidate planets, especially those larger than Neptune. Third, because metal-poor stars are smaller, stars with detected planets will be very slightly (<0.02 dex) more metal-poor than the target average. Fourth, uncertainties in stellar radii produce correlated errors in planet radius and stellar irradiation. A previous finding, that highly-irradiated giant are more likely to have “inflated” radii, remains significant, even accounting for this effect. In contrast, transit depth is negatively correlated with stellar metallicity even in the absence of any intrinsic correlation, and a previous claim of a negative correlation between giant planet transit depth and stellar metallicity is probably an artifact.

13

Subject headings: Planetary systems — Planets and satellites: detection — Stars:

14

fundamental parameters — Methods: statistical

1. Introduction

When an exoplanet’s orbital plane lies along our line of sight, the planet will transit its host star, periodically obscuring a small portion of the stellar disk and producing detectable dips in a photometric lightcurve. The first transits (of a planet previously discovered by Doppler) were observed in 1999 (Henry et al. 2000; Charbonneau & Brown 2000). The first exoplanet to be detected with the transit technique was confirmed by Doppler observations in 2002 (Konacki et al. 2003). As of 18 October 2012, 288 confirmed transiting planets in 233 systems have been reported (Schneider et al. 2011). The *Kepler* mission, operating since 2009, has identified more than 2300 candidate transiting planets (*Kepler* Objects of Interest or KOIs) (Batalha 2012, hereafter B12). Although only a small fraction of KOIs have been confirmed, the false positive rate is thought to be low (Morton & Johnson 2011; Lissauer et al. 2012), but see Santerne et al. (2012).

Transit searches are more sensitive than Doppler searches to the smallest planets because the transit signal scales with the square of the planet radius R_p , while the Doppler signal of a rocky planet scales approximately as R_p^4 (Valencia et al. 2007). *Kepler* has already discovered 90 candidates possibly *smaller* than Earth. Transiting planets are of special interest because their radii can be estimated from the transit signal. If the transit is not grazing, the fractional decrease δ in the star’s observed flux is

$$\delta = \left(\frac{R_p}{R_*} \right)^2, \quad (1)$$

where R_* is the stellar radius. A measurement of δ combined with knowledge of R_* yields the planet radius. Because the inclination of a transiting planet’s orbit is near 90° , the mass of the planet can also be unambiguously established from Doppler observations. Combinations of mass and radius can be compared with predictions by models of interior structure (Seager et al. 2007; Grasset et al. 2009; Rogers et al. 2011). Spectroscopy or spectrophotometry during transits can detect or rule out constituents in an atmosphere

39 (Charbonneau et al. 2002; Bean et al. 2010; Désert et al. 2011), and secondary eclipses
40 (occultations of the planet) can constrain temperature and albedo (Charbonneau et al.
41 2005; Knutson et al. 2008; Rowe et al. 2008). Additional planets can be discovered by
42 variation in transit times (Agol et al. 2005; Ford et al. 2011).

43 Analyses of large samples of transiting planets, including the catalog of KOIs, have
44 attempted to ascertain properties of transiting planet populations, e.g., whether they are
45 segregated into discrete groups (Fressin et al. 2009), the distribution with planet radius
46 (Howard et al. 2012) the dependence of planet occurrence on the metallicity of the host
47 star (Schlaufman & Laughlin 2011; Buchhave et al. 2012), the effect of stellar irradiance
48 on giant planet radius (Demory & Seager 2011; Enoch et al. 2012), and the occurrence
49 of planets compared to Doppler surveys (Gaidos et al. 2012; Wolfgang & Laughlin 2012;
50 Wright et al. 2012). In the case of *Kepler*, lack of Doppler confirmation for most candidate
51 planets as well as detailed spectroscopic characterization of the stars make it important to
52 properly account for any systematic effects or biases.

53 Detection of a planet in a transit survey depends on the properties of the planet,
54 most notably R_p (Equation 1), but also on the orbital period because it determines the
55 number of transits that are observed and the total transit signal. Gaudi (2005), Gaudi et al.
56 (2005), and Pont et al. (2006) pointed out that transit-selected samples are biased toward
57 large planets on short-period orbits. These biases can be extreme in ground-based surveys
58 which suffer correlated (“red”) noise from variations in atmospheric transmission and
59 discontinuous observing windows.

60 Equation 1 also shows that planets of a given radius will be more readily detected
61 around smaller stars. This has, in part, motivated transit searches for planets around M
62 dwarf stars (Tarter et al. 2007; Gaidos et al. 2007; Charbonneau & Deming 2007). In this
63 case, a property of the host star, as opposed to the planet, influences the likelihood that

64 a transiting planet will be detected, and that both star and planet will be included in a
65 transit-selected sample. Thus a selection effect will act on stellar radius, or on any property
66 that is related to stellar radius, such as metallicity. This will produce systematic offsets or
67 biases in the properties of stars hosting known transiting planets relative to the properties
68 of the target sample.

69 The construction of a target catalog itself can also produce selection effects in a transit
70 survey. Most notable among constraints on target stars is an apparent magnitude limit
71 because of a signal-to-noise ratio (SNR) requirement, or the need to confirm candidate
72 transiting systems using Doppler observations. A magnitude limit will cause (Malmquist)
73 bias towards more luminous stars; these can be included to larger distances and hence
74 sample a larger volume of space. At a given effective temperature, luminosity is uniquely
75 related to stellar radius, and hence this is also a bias towards larger stars that, unmitigated,
76 will affect the detection of planets and estimates of their radii.

77 Some of these effects would disappear or could be corrected if stellar parameters,
78 i.e. radius, were precisely established. But, up to now, the large scale of transit surveys
79 ($10^4 - 10^7$ stars) has precluded such determinations. Neither radius nor mass are directly
80 observable for distant, single stars such as *Kepler* targets. The properties of most *Kepler*
81 stars have been inferred by comparing stellar models to the broad-band photometry of the
82 *Kepler* Input Catalog (KIC) (Brown et al. 2011, hereafter Br11). Few spectra and almost
83 no parallax (distance) measurements are available, and most stars have only upper limits
84 on proper motion. KIC estimates of stellar radii have large uncertainties due to (i) errors in
85 photometry; (ii) degeneracies between stellar parameters and colors; and (iii) errors in the
86 models themselves. While KIC estimates of stellar effective temperature are comparatively
87 robust, those of surface gravity ($\log g$) and metallicity (Fe/H) are not as reliable (Br11).
88 Br11 concluded that no gravity or radius information could be inferred for stars hotter than

89 5400 K ($g - r < 0.65$). Verner et al. (2011) found that the KIC and astroseismic radii of 500
90 solar-type stars have random discrepancies of order 50% and a systematic offset of about
91 the same amount. Bruntt et al. (2012) found a similar scatter but negligible systematic
92 offset in $\log g$ (and hence the radius) of 93 solar-type *Kepler* stars. Mann et al. (2012) found
93 that many M-type stars that were classified as dwarfs or were unclassified in the KIC are
94 actually evolved stars.

95 Selection effects acting on uncertainties in stellar radius will bias the observed
96 properties of planet-hosting stars with respect to their true distributions. For example,
97 while essentially all M-type hosts of KOIs are *bona fida* dwarf stars (Muirhead et al.
98 2012), the vast majority of the bright ($K_p < 14$) targets and some fainter stars are giants
99 (Mann et al. 2012). This disparity is a result of the strong selection effect on stellar radius
100 described above; planets are far more difficult to detect around giant stars due to their
101 large size and higher variability (Huber et al. 2010). Because of the relation between planet
102 radius and stellar radius (Equation 1), estimates of planet radius will likewise be affected.

103 Here, we quantify five effects produced by selection bias and uncertainties in stellar
104 parameters in the *Kepler* survey. In Section 2 we derive useful scaling relationships for
105 selection effects on transiting planet detection and target star selection. In Section 3 we
106 apply these concepts to the *Kepler* survey using the KOI catalog, parameters from the
107 KIC, and models of stellar evolution and stellar populations. We describe our methods
108 and models in Section 3.1. In Section 3.2, we calculate the effect of Eddington bias on
109 the radius distribution of KOIs as a result of uncertainties in stellar radius. In Section 3.3
110 we describe the effect of Malmquist bias on the magnitude-limited *Kepler* target catalog
111 and the preferential inclusion of more luminous, larger stars, thus biasing downwards
112 the radius of some KOIs. In Section 3.4 we estimate the bias towards lower metallicity
113 among KOI-hosting stars as a consequence of the relationship between stellar metallicity

114 and radius on the main sequence. In Section 3.5 we describe how uncertainties in stellar
 115 radius produce correlated errors in planet radius and stellar luminosity, potentially
 116 affecting statistics describing the relationship between “inflated” giant planets and stellar
 117 irradiation. In Section 3.6 we consider the effect of stellar metallicity on transit depth and
 118 the interpretation of any correlation between metallicity and the radii of giant planets.
 119 We summarize our results and describe current and future efforts to better determine the
 120 parameters of *Kepler* stars in Section 4.

121 2. Analytical scaling relations

122 In a transit survey, selection bias acts on a quantity X (a stellar or planetary
 123 parameter) when the probability f that a star is included in the survey, or that a planet is
 124 detected transiting a star, depend on that parameter. This bias is superposed on any real
 125 correlations and will persist to the extent that the values of the parameter and its effect on
 126 inclusion or detection are imperfectly quantified. The bias δX is the difference between the
 127 observed mean $\langle Xf \rangle / \langle f \rangle$ and the intrinsic mean $\langle X \rangle$, or

$$\delta X = \frac{\langle Xf \rangle - \langle X \rangle \langle f \rangle}{\langle f \rangle}, \quad (2)$$

128 where the brackets represent marginalizing over the population of stars, subject to any
 129 constraints. To derive useful scaling relations, we chose apparent brightness (magnitude)
 130 and effective temperature T_e as independently varying parameters. The first fixes the
 131 noise level against which a transit must be detected. Moreover, the *Kepler* target catalog is
 132 magnitude-limited (Batalha et al. 2010). Among main sequence stars, T_e is closely related
 133 to mass, an important parameter of planet populations (Johnson et al. 2010; Howard et al.
 134 2012). Unlike other stellar parameters, it can be robustly estimated from KIC photometry
 135 (Br11, Pinsonneault et al. 2012)). Effective temperature is thus a convenient plotting
 136 parameter which minimizes complications due to variation in the planet population along

137 the main sequence. Nevertheless, values of T_e do *not* map to unique values of stellar mass
 138 because stars have different ages and metallicities and plots with T_e the dependence on
 139 mass should be considered “blurred”. Calculations using stellar models, as described below,
 140 explicitly take into account the effects of age and metallicity.

141 2.1. Selection bias due to transit detection

142 We first estimate the probability f that a star is included in a catalog of transiting
 143 systems. The probability of detecting a planet is calculated as a function of both stellar
 144 properties (radius and mass R_* and M_*) and planet properties (radius R_p and orbital
 145 period P), and then marginalized over planet properties using an appropriate distribution
 146 function. This yields f as a function of R_* and M_* . Equation 2 can then be evaluated using
 147 a stellar model that describes the intrinsic distributions of these parameters and their
 148 relations to other observables. In many instances we can use scaling relations rather than
 149 exact relations because Equation 2 is normalized.

150 We adopted a double power-law for the intrinsic distribution f' of planets with
 151 radius and orbital period (Cumming et al. 2008; Howard et al. 2010; Mayor et al. 2011;
 152 Howard et al. 2012):

$$df' \sim R_p^{-\alpha} P^{-\beta} d \ln R_p d \ln P, \quad (3)$$

153 for P larger than some minimum value P_{min} where planets are found. Transit detection
 154 depends on the geometric probability that the planet is on a transiting orbit, as well as the
 155 the signal (depth) of the transit relative to noise.

156 In the absence of coherent or “red” noise from the atmosphere, the signal-to-noise ratio
 157 of a single transit is $\sqrt{N} (R_p/R_*)^2$, where N is the total number of photons detected during
 158 the event. In an observation interval t about t/P transits will be observed, bringing the

159 total number of photons to $\sim Nt/P$. Therefore the signal-to-noise ratio of the co-added
 160 transits is

$$\text{SNR} = \sqrt{\frac{Nt}{P}} \left(\frac{R_p}{R_*} \right)^2. \quad (4)$$

161 At a given apparent brightness, $N \sim \tau$, where τ is the transit duration. When the transit
 162 impact parameter is low and the transit chord is close to the stellar diameter, $\tau \approx 2R_*/V$.
 163 Assuming a near-circular orbit, the transverse velocity V can be expressed in terms of the
 164 orbital period and mass of the star and

$$\tau \approx 2R_* \left(\frac{P}{2\pi GM_*} \right)^{1/3}, \quad (5)$$

165 where G is the gravitational constant. We derive a scaling relation between SNR and
 166 planet/star properties by substituting τ for N in Equation 4 and ignoring constant factors:

$$\text{SNR} \sim R_p^2 P^{-1/3} R_*^{-3/2} M_*^{-1/6}. \quad (6)$$

167 Solving for R_p gives a scaling relation for the radius of the smallest planet on a given orbital
 168 period that can be detected at a fixed SNR threshold:

$$R_{min} \sim R_*^{3/4} M_*^{1/12} P^{1/6}. \quad (7)$$

169 Likewise, there is a relation for the maximum orbital period at which a planet of a given
 170 radius R_p can be detected at a fixed SNR threshold:

$$P_{max} \sim R_p^6 R_*^{-9/2} M_*^{-1/2}. \quad (8)$$

171 P_{max} is a sensitive function of R_p , underscoring why transit surveys are highly biased
 172 towards the largest planets (Gaudi 2005).

173 To obtain the observed distribution f of planets with R_* and M_* , we multiply the
 174 intrinsic distribution (Equation 3) by the geometric probability that a planets is on a
 175 transiting orbit. For circular orbits this is proportional to the ratio of the stellar radius

176 to orbital semimajor axis R_*/a which, based on Newtonian orbital dynamics, scales as
 177 $R_* M_*^{-1/3} P^{-2/3}$. The observed planet distribution is:

$$df \sim R_* M_*^{-1/3} R_p^{-\alpha} P^{-(\beta+2/3)} d \ln R_p d \ln P, \quad (9)$$

178 We marginalize Equation 9 over both P and R_p , first integrating from P_{min} to P_{max} . The
 179 maximum period is also limited by the observing window and the requirement that more
 180 than one transit must be observed, e.g. $P_{max} \leq t/3$.

181 Integration of $P^{-(\beta+2/3)} d \ln p$ in Equation 9 yields a factor proportional to
 182 $P_{min}^{-(\beta+2/3)} - P_{max}^{-(\beta+2/3)}$. If $P_{min} \ll t$, then Equation 8, is used to re-express this as
 183 $P_{min}^{-(\beta+2/3)} [1 - (R_p/R_m)^{-(6\beta+4)}]$, where R_m is the radius of the smallest planet that can be
 184 detected at $P = P_{min}$, i.e. that can be detected at all). Integration of Equation 9 over R_p
 185 from R_m to ∞ produces:

$$\int df \sim R_* M_*^{-1/3} R_m^{-\alpha} P_{min}^{-(\beta+2/3)} \int_1^\infty x^{-(\alpha+1)} (1 - x^{-(6\beta+4)}) dx, \quad (10)$$

186 were $x \equiv R_p/R_m$. Because the P_{min} factor and the integral depend only on α and β , which
 187 are planet population parameters and not stellar properties, they can be ignored when
 188 calculating biases in stellar properties. Substituting for R_m and retaining only factors that
 189 depend on stellar properties,

$$f \sim R_*^{1-3\alpha/4} M_*^{-(1/3+\alpha/12)} \quad (11)$$

190 All else being equal, planets are more likely to be detected around stars with smaller radii
 191 (because transit depths are larger) and/or lower masses (because transit durations are
 192 longer). Smaller stars are thus more likely to appear in a transit-selected sample. In the
 193 case of mass-radius relation $R_* \sim M_*^{0.8}$ for zero-age solar-type stars (Cox 2000) and a planet
 194 radius distribution power-law index $\alpha = 2.6$ (Howard et al. 2012), then $f \sim M_*^{-1.31}$. This
 195 is simply a statement that smaller (and more) planets can be detected around lower mass
 196 stars. Older stars will have a steeper mass-radius relation, and as a result the dependence
 197 of f on M_* will be more pronounced.

198 At a given apparent brightness (observed flux), the quantity BR_*^2/d^2 is fixed, where
 199 B is the stellar surface brightness in the bandpass of interest and d is the distance to the
 200 star. Substituting, $R_* \sim d/\sqrt{B}$ into Equation 11, and assuming that the planet population
 201 is distance-independent so that the distance factor can be moved outside the period and
 202 radius integrals, the scaling relation for observed occurrence becomes:

$$f \sim d^{1-3\alpha/4} B^{3\alpha/8-1/2} M_*^{-(1/3+\alpha/12)}. \quad (12)$$

203 If $\alpha > 4/3$, (Howard et al. 2012, e.g.), closer and hotter host stars are more likely to
 204 be included in transit-selected samples. Stellar age and metallicity, which affect the
 205 relationships between stellar mass, radius, and surface brightness, are also biased as a
 206 result. A correlation between stellar properties and distance can modulate the degree of this
 207 bias. For example, if more distant stars tend to be more evolved along the main sequence
 208 and thus hotter, the bias will be less than if d and B are independent. Equation 12 does
 209 not consider that star of a certain mass or radius may be *over-represented* in the parent
 210 population: this is discussed in the next section.

211 2.2. Selection bias due to target selection

212 The target catalogs of transit surveys such as *Kepler* are selected using a number of
 213 criteria, and chief among these is apparent magnitude. A magnitude-limited sample of stars
 214 will be biased towards the most luminous objects, which will be included to greater distances
 215 (Malmquist 1922). These stars may be either more massive, more evolved, or both. At
 216 a given T_e and thus fixed surface brightness B (ignoring the weak dependence of surface
 217 brightness on gravity and metallicity), the signal N from a star during a transit will scale
 218 as $(R_*/d)^2$. Modifying Equation 4 appropriately, we find that the transit signal-to-noise
 219 ratio scales as

$$\text{SNR} \sim R_p^2 P^{-1/3} R_*^{-1/2} M_*^{-1/6} d^{-1}. \quad (13)$$

220 The smallest planet that can be detected at a given SNR will scale as

$$R_{small} \sim P^{1/6} R_*^{1/4} M_*^{1/12} d^{1/2}. \quad (14)$$

221 Multiplying a power-law distribution of planet radii (Equation 3) by the probability that a
 222 planet is on a transiting orbit ($\sim M_*^{-1/3} R_*$) and integrating over all planet radii down to
 223 R_{small} gives the relation

$$f \sim P^{-\alpha/6} R_*^{1-\alpha/4} M_*^{-(1/3+\alpha/12)} d^{-\alpha/2}. \quad (15)$$

224 At a fixed color/temperature/surface brightness B , a magnitude-limited survey will include
 225 stars of radius R_* out to a distance $d_{max} \sim R_*$. Assuming, for the moment, that transits can
 226 be detected to arbitrarily large distances, then integrating Equation 15 over a homogeneous
 227 volume of radius d_{max} yields

$$f \sim P^{-\alpha/6} R_*^{4-3\alpha/4} M_*^{-(1/3+\alpha/12)}. \quad (16)$$

228 For $\alpha = 2.6$ and at a given P , f scales as $R_*^{2.05} M_*^{-0.55}$. This relation illustrates how larger,
 229 more evolved stars can be preferentially included in a transit-selected sample despite the
 230 fact that transits of these stars are more difficult to detect.

231 Although target stars in a magnitude-limited sample will be included to a distance
 232 $d_{max} \sim R_*$, a planet of radius R_p can only be detected to a distance d_{det} where, according
 233 to Equation 13,

$$d_{det} \sim R_p^2 P^{-1/3} R_*^{-1/2} M_*^{-1/6}. \quad (17)$$

234 The detection limit decreases with R_* while the inclusion limit d_{max} increases with R_* .
 235 These limits coincide ($d_{max} = d_{det}$) at a stellar radius \tilde{R}_* :

$$\tilde{R}_* = \tilde{R}_0 R_p^{4/3} P^{-2/9} M_*^{-1/9}, \quad (18)$$

236 where \tilde{R}_0 is a constant factor, P is in days, R_p is in Earth radii and M_* is in solar masses.
 237 (We calculate values of \tilde{R}_0 for the *Kepler* survey in Section 3.3.) Detections of planets

238 of a given size around stars with $R_* < \tilde{R}_*$ is magnitude-limited and subject to a stellar
 239 radius bias that scales as $\sim R_*^4$, because the sample volume increases as R_*^3 and the transit
 240 probability increases as R_* . For stars with $R_* > \tilde{R}_*$, a survey is limited to a volume
 241 proportional to $d_{det}^3 \sim R_*^{-3/2}$ (see Equation 14), and the bias scales as $\sim R_*^{-1/2}$, a weak
 242 dependence on R_* in the opposite sense. The critical stellar radius \tilde{R}_* is most sensitive to
 243 planet radius and the dependence on period and stellar mass is weak.

244 3. Application to the *Kepler* transit survey

245 3.1. Methods

246 To evaluate biases and selection effects in the *Kepler* survey we modeled target stars
 247 with isochrones from the Dartmouth Stellar Evolution Database (Dotter et al. 2008)
 248 interpolated onto a 0.1-dex grid of metallicities using the on-line tool. For each star, we
 249 compared adjusted KIC parameters ($T \equiv T_e$, $\mathcal{G} \equiv \log g$, $\mathcal{F} \equiv [\text{Fe}/\text{H}]$) to model predictions
 250 using Bayesian statistics. Specifically, we calculated a probability or weight w for each
 251 model according to:

$$w = e^{-\left[\frac{(T-\hat{T})^2}{2\sigma_T^2} + \frac{(\mathcal{G}-\hat{\mathcal{G}})^2}{2\sigma_{\mathcal{G}}^2} + \frac{(\mathcal{F}-\hat{\mathcal{F}})^2}{2\sigma_{\mathcal{F}}^2}\right]} p(M_*)p(t_*)p(\mathcal{F})p(\zeta), \quad (19)$$

252 where parameters with a “hat” are the Dartmouth model values and $p(M_*)$, $p(t_*)$, $p(\mathcal{F})$,
 253 and $p(\zeta)$ are the priors for initial stellar mass (initial mass function, IMF), age, metallicity,
 254 and a modified distance modulus $\zeta \equiv \mu + 5 \log_{10} \sin b$, where b is the galactic latitude.
 255 The modified distance modulus accounts for the finite dispersion of stars above the plane
 256 of the Milky Way, but neglects the vertical displacement of the Sun. We used an SDSS
 257 r -band modulus $\mu = m_r - M_r$, where m_r is the observed apparent magnitude and M_r is the
 258 absolute magnitude from the Dartmouth models. We ignored interstellar extinction, which
 259 will be < 0.5 magnitudes (Schlegel et al. 1998). (While estimation of stellar parameters is

260 sensitive to interstellar *reddening*, the amount of interstellar *extinction* is small compared to
 261 the uncertainties in the distance modulus.) Estimates of T_e and $[\text{Fe}/\text{H}]$ from the KIC were
 262 adjusted by -100 K and 0.17 dex, respectively and we used $\sigma_{T_e} = 200$ K, $\sigma_{\log g} = 0.36$ dex,
 263 and $\sigma_{\text{Fe}} = 0.3$ dex, based on a comparison of KIC values with those spectroscopic values
 264 listed in B12.

265 For priors we adopted the Kroupa (2002) IMF, and a uniform age distribution over
 266 1-13 Gyr. The latter corresponds to a constant rate of star formation since the advent of
 267 the galactic disk (Oswalt et al. 1996; Liu & Chaboyer 2000), but ignores the youngest stars,
 268 around which planets are more difficult to detect. The metallicity distribution of *Kepler*
 269 target stars is unknown and may be complex; the field is not parallel to the Galactic plane
 270 and may include members of a metal-poor “thick disk” population (Ruchti et al. 2011). We
 271 used the metallicity distribution predicted by the the TRILEGAL stellar population model
 272 (Vanhollebeke et al. 2009) as a prior. Stars in the direction of the center of the *Kepler* field
 273 ($\ell = 76.32^\circ$, $b = 13.5^\circ$) were simulated to a cutoff magnitude $K_P = 16$. When compared
 274 to 2MASS counts, TRILEGAL counts agree with observations at least down to $b = 10^\circ$,
 275 but fail at $b = 0$, possibly due to incorrectly modeled bulge red giant branch stars and dust
 276 (Girardi et al. 2005). However, the Kepler field cuts off at $b = 6^\circ$ and only 18 of the 84
 277 CCD centers lie at $b < 10^\circ$. The (mostly default) values for TRILEGAL parameters are
 278 listed in Table 1.

279 TRILEGAL also reports a value of μ for each simulated star and we used these to
 280 construct a prior distribution of ζ . Our priors are relaxed in the sense they only exclude
 281 very unlikely masses, ages, or metallicities. It is also possible to impose priors on the stellar
 282 parameters T_e and $\log g$ using the predictions of a stellar population model, but we consider
 283 such predictions too uncertain to justify this approach.

284 For each star, Equation 19 returns an array of values for w corresponding to the grid

285 of Dartmouth models. Most values of w are negligibly small and the corresponding models
 286 were ignored. From the remainder, the most probable (highest w) model and accompanying
 287 parameters such as R_* were identified. Statistics of the distribution of possible values were
 288 calculated, e.g:

$$\bar{R}_* = \frac{\sum_i w_i R_*(i)}{\sum_i w_i}. \quad (20)$$

289 Because the distributions can be very non-gaussian, we defined the fractional uncertainty
 290 in a stellar parameter to be one-half of the range encompassing 68% of the total probability
 291 (normalized w) divided by the most probable value. We found that uncertainties in
 292 the radii of late G- and K-type dwarf stars hosting KOIs is typically $\sim 15\%$, but are
 293 substantially higher ($\sim 100\%$) among some F- and G-type stars because of the coincidence
 294 of the dwarf and (sub)giant branches (Figure 1). Evolved stars (i.e. KIC $\log g < 4$) also
 295 have comparatively larger uncertainties. The cluster of putative M “dwarfs” with radius
 296 uncertainties of $\sim 25\%$ might be misclassified giant stars (Mann et al. 2012). Our estimated
 297 uncertainties are certainly lower bounds because (1) the errors in the stellar parameters
 298 T_e , $[\text{Fe}/\text{H}]$, and especially $\log g$ are themselves not gaussian-distributed, as presumed in
 299 Equation 19; and (2) we do not consider errors in the Dartmouth models themselves.

300 3.2. Eddington Bias

301 Eddington bias occurs when errors in measurement scatter more frequent values
 302 in a population to less frequent values at a higher rate than the reverse process. This
 303 systematically inflates the observed frequency of rare members (Eddington 1913). Because
 304 the distribution of planets with radius is a steep power law (Cumming et al. 2008;
 305 Howard et al. 2010; Mayor et al. 2011; Howard et al. 2012), errors in radius (fractional
 306 standard deviation σ_R) will bias the number of larger planets upwards. This will inflate the
 307 rate of planet occurrence f above a given cutoff in radius R_C . Planets with radius R_P will

308 appear to be larger than the cutoff if the error in stellar radius is larger than $R_C/R_P - 1$.
 309 If errors in stellar radius are gaussian-distributed, the fraction of stars that satisfy that
 310 condition is $\text{erfc}((R_C/R_P - 1)/(\sqrt{2}\sigma_R)) / 2$. The fractional upward bias in planet occurrence
 311 is the integral of this function with the normalized planet radius distribution, minus the
 312 intrinsic occurrence (normalized to unity):

$$\Delta f = \frac{\alpha}{2} \int_0^\infty x^{-(\alpha+1)} \text{erfc}\left(\frac{x^{-1} - 1}{\sqrt{2}\sigma_R}\right) dx - 1, \quad (21)$$

313 where $x \equiv R_p/R_C$. Δf increases with σ_R and, if $\alpha = 2.6$, reaches 18% when $\sigma_R = 30\%$.

314 We estimated the amount of Eddington bias in the apparent radius distribution of KOIs
 315 using the procedures described in Section 3.1. For each KOI we calculated the likelihood
 316 weight w (Equation 19) for all possible stellar models consistent using the parameters of the
 317 host star. Corresponding to each model we calculated a revised planet radius $R_p \times (R'_*/R_*)$,
 318 where R_p is the radius from B12, R'_* is the model stellar radius and R_* is the stellar radius
 319 of the maximum likelihood model (highest w). The radius distribution, weighted by w ,
 320 is summed over all KOI host stars and normalized. This is compared to the observed
 321 distribution of R_p (Figure 2). The latter is not the *intrinsic* distribution, which must
 322 account for the probability that a planet transits and is detected (Howard et al. 2012).
 323 As expected, Eddington bias increases the apparent number of Neptune-size and larger
 324 planets. The bias is 17% above $3.4R_\oplus$, demarcated by the vertical dashed line in Figure
 325 2, where the normalized distributions are equal. The bias also suppresses the peak in the
 326 distribution at a Jupiter radius. Corollaries of these results are that the actual occurrence
 327 rate of Neptune-size planets is smaller than previously reported (Howard et al. 2012, i.e.),
 328 and that the intrinsic peak at $R_p \sim 1R_J$ is more pronounced than is apparent.

329 In addition, Eddington bias decreases the apparent slope in the radius distribution
 330 (Figure 2). This is a consequence of the observed turnover in the number of planets smaller
 331 than $\sim 2R_\oplus$, and whether more large planets are scattered to smaller radii than vice

332 versa. *Kepler* observations are incomplete for $R_P < 2R_\oplus$ and while the intrinsic radius
 333 distribution of planets is presumed to turn over, the radius at which this actually occurs is
 334 not known and awaits a better understanding of the efficiency of *Kepler* detection of small
 335 signals. If the turnover below $2R_\oplus$ is real, then the intrinsic slope of the radius distribution
 336 is *steeper* than observed ($\alpha = 2.6$). But if a scale-free power-law distribution continues to
 337 much smaller radii, then Eddington bias affects the magnitude, but not the slope of the
 338 distribution.

339 We simulated Eddington bias on artificial samples of planets with radii drawn from a
 340 power-law distribution with variable index α . These radii replaced actual KOI estimates
 341 in a repeat of the analysis described above. The power-law index of the binned apparent
 342 distribution $\rho(R_i)$ above some minimum radius R_{min} is calculated by maximum likelihood:
 343 $\alpha = \sum_i \rho(R_i) / \sum_i \rho(R_i) \log(R_i/R_{min})$, where the summation is over all $R_i > R_{min}$. As
 344 expected, while Eddington bias significantly increases the fraction of planets with $R > R_{min}$,
 345 the power-law index is relatively unchanged (Figure 3).

346 3.3. Malmquist Bias

347 Malmquist bias is the preferential inclusion of intrinsically luminous objects in a
 348 magnitude-limited survey due to the rapid increase in sampling volume d_{max}^3 with distance
 349 d_{max} to which an object is included. Among large, readily-detected objects (planets) in a
 350 magnitude-limited transit survey, the bias is even greater ($\sim d_{max}^4$) because the probability
 351 of a transiting geometry is proportional to R_* which, at a given effective temperature, scales
 352 with d_{max} (see Section 2.2). At a given apparent magnitude and planet radius, there is a
 353 maximum stellar radius \tilde{R}_* to which a survey is essentially complete, i.e. not limited by the
 354 SNR of a transit event.

355 We estimated \tilde{R}_* as a function of R_p by establishing the detection limit at different
 356 *Kepler* magnitudes. The *Kepler* target catalog was constructed with different criteria
 357 for stars with $K_p < 14$ and $14 < K_p < 16$ (Batalha et al. 2010); it is probably nearly
 358 complete for dwarf stars to $K_p = 14$ but only includes selected dwarfs with $14 < K_p < 16$
 359 (Batalha et al. 2010). We adopted a SNR limit of 7.1 and an observation period of 487 d
 360 (B12). To estimate the noise of a typical dwarf star we performed a polynomial fit to a
 361 running median ($N = 1000$) of 3 hr combined differential photometric precision (CDPP)
 362 values for *Kepler* targets with $\log g > 4$, presumed mostly dwarfs. This gave an estimate of
 363 the intrinsic 3 hr RMS noise level as a function of K_p ;

$$\log \sigma_3(\text{dwarfs}) \approx -4.27 + 0.116(K_p - 12) + 0.0247(K_p - 12)^2. \quad (22)$$

364 The median noise at $K_p = 12$ is 54 ppm. We performed a similar analysis on stars with
 365 KIC $\log g < 4$, presumably subgiants and giants, that constitute a locus of comparatively
 366 “noisy” targets, and found:

$$\log \sigma_3(\text{giants}) \approx -3.69 + 0.045(K_p - 12) + 0.115(K_p - 12)^2. \quad (23)$$

367 For $K_p = 14$ dwarfs, $\tilde{R}_0 = 1.72R_\odot$ and at $K_p = 16$, $\tilde{R}_0 = 0.77R_\odot$. At $K_p = 14$, for a
 368 median orbital period $P \approx 16$ d and $R_p = 2R_\oplus$, Malmquist bias favors stars as large as
 369 $2.3R_\odot$. At $K_p = 16$, only stars with $R_* < 1.0R_\odot$ are favored because of higher noise at
 370 fainter magnitudes. The situation is more extreme for giant planets ($R_p \sim 10R_\oplus$), where
 371 Malmquist bias will favor evolved stars as large as $10\text{-}20R_\odot$, presuming giant planets exist
 372 around such stars, as we discuss below.

373 Bias towards larger stars, coupled with uncertainties in stellar radius, leads to
 374 underestimates of stellar - and hence planetary - radii. We quantified this effect using the
 375 machinery described in Section 3.1, with the addition of a Malmquist bias factor. For each
 376 KOI-hosting star, we evaluated the mean stellar radius by averaging over all stellar models

377 weighted by w (from Equation 19) and multiplied by either $(R_*/\tilde{R}_*)^4$, where $R_* < \tilde{R}_*(P, K_p)$,
 378 or $(R_*/\tilde{R}_*)^{-1/2}$, if $R_* < \tilde{R}_*(P, K_p)$.

379 The ratio of the “naive” mean model radius to the bias-weighted mean radius is plotted
 380 in Figure 4 vs. the nominal planet radius published in B12. Deviation of this factor from
 381 unity can be considered the error in radius that results if Malmquist bias is not taken into
 382 account. About two-thirds of all KOI-hosting stars, and the vast majority of those hosting
 383 planets smaller than Neptune have predicted Malmquist bias values $<10\%$. However, the
 384 majority of larger planets may have significantly underestimated radii, some by a factor
 385 of two. This dichotomy occurs because *Kepler* detection of large planets is limited by the
 386 magnitude limit of the target catalog, not the SNR of transit. We emphasize that these
 387 calculations are *statistical*, i.e. we are calculating the expectation values of probability
 388 distributions with stellar radius, and that actual errors will vary. Nevertheless, the host
 389 stars of many giant planets may be more larger, more distant, and more luminous, and
 390 the radii of their planets may be significantly underestimated. Inclusion of larger, evolved
 391 stars means that some KOIs may be astrophysical false positives, e.g. M dwarf companions
 392 masquerading as planets (Charbonneau et al. 2004; Almenara et al. 2009), a possibility
 393 that we discuss in Section 4.

3.4. Metallicity Bias

394
 395 The metallicity of host stars is an important parameter in studies of planet statistics.
 396 A correlation between stellar metallicity and the presence of giant planets has been
 397 unambiguously established (Gonzalez 1998; Santos et al. 2004; Fischer & Valenti 2005;
 398 Buchhave et al. 2012) and is consistent with a prediction by the core-triggered instability
 399 theory of giant planet formation (Mizuno 1980), i.e. that a solid core that initiates runaway
 400 accretion before the gas dissipates is more likely to form in a disk with a higher abundance

401 of solids. Doppler surveys have failed to find any correlation between metallicity and the
 402 occurrence of Neptune-size or smaller planets (Sousa et al. 2008; Mayor et al. 2009, 2011).
 403 Schlaufman & Laughlin (2011) found that the average $g-r$ color of most *Kepler* stars with
 404 small candidate planets was no different from the average of all stars at a given $J-H$ color,
 405 except for late K and early M-type stars; those with planets have redder $g-r$ colors and
 406 Schlaufman & Laughlin argued that these are more metal-rich. However, this difference
 407 may be an artifact of contamination of the sample by evolved stars, which have bluer $g-r$
 408 colors than dwarfs and make the overall sample, but not the KOI-hosting sample, bluer
 409 (Mann et al. 2012). Indeed, $g-r$ color might be insensitive to or depend only weakly on
 410 metallicity for these spectral types (Lepine et al. 2012). Muirhead et al. (2012) report
 411 metallicities of 78 late K and M dwarfs with KOIs based on infrared spectra. The mean
 412 value, -0.09 , is consistent with the metallicity of M dwarfs in the solar neighborhood
 413 (Schlaufman & Laughlin 2010; Woolf & West 2012). The average metallicity of *Kepler* M
 414 dwarfs is not known but these intrinsically faint stars are within a few hundred pc of the
 415 Sun (Gaidos et al. 2012).

416 The metallicities of stars of transiting planets need not be representative of the
 417 underlying population of planet-hosting stars. Metals are an important source of opacity in
 418 the atmospheres of cool stars, and, all else being equal, metal-poor dwarf stars should have
 419 smaller radii. A transiting planet will be more detectable around a metal-poor subdwarf
 420 than a metal-rich dwarf star, and thus the host stars of KOIs will be biased towards
 421 metal-poor representatives of the overall population. If sufficiently large, this bias could
 422 obfuscate any intrinsic relationship between stellar metallicity and the presence of planets.

423 We calculated the metallicity bias, i.e the expected metallicity of stars with detected
 424 transiting planets minus the expected metallicity, for all *Kepler* Quarter 6 target stars
 425 using Eqns. 2 and 11, and the methods described in Section 3.1. The difference between

426 the “naive” mean metallicity of Dartmouth models for each star, and the biased mean
 427 using the factor of Equation 11, is plotted vs. adjusted KIC effective temperature in
 428 Figure 5. As expected, the metallicity bias is negative except for a locus of positive values
 429 corresponding to evolved stars, for which radius *decreases* with increasing metallicity, e.g.
 430 Zielinski et al. (2012). The bias is small (mean of -0.017 among dwarfs) for the following
 431 reasons: (i) the geometric transit probability is proportional to stellar radius and thus
 432 increases with metallicity, countering the effect of metallicity on transit depth; and (ii)
 433 the effect of metallicity on stellar radius is most pronounced among comparatively rare
 434 subdwarfs but has only a modest effect around solar metallicity, especially for the coolest
 435 stars (Boyajian et al. 2012).

436 3.5. Covariant errors and “inflated” Jupiters

437 At the time the first exoplanet around a main sequence star was confirmed,
 438 Guillot et al. (1996) realized that highly-irradiated giant planets on close-in orbits may
 439 have anomalously large radii. After sufficient numbers of transiting giant planets were
 440 discovered, it became apparent that some were “inflated” compared to theoretical
 441 predictions (Burrows et al. 2000; Baraffe et al. 2003). Planets larger than $R_J \approx 1.2$ cannot
 442 be explained by conventional interior models of gas giants and require an additional source
 443 of internal energy to inflate them (Fortney et al. 2010). Several non-exclusive explanations
 444 for the requisite energy source have been put forward (Bodenheimer et al. 2001; Showman
 445 2002; Batygin & Stevenson 2010). One important clue is that planets experiencing higher
 446 irradiance or having higher emitting temperature are more likely to be inflated. Correlations
 447 between equilibrium temperature and radius have been reported among transiting giant
 448 planets discovered in ground-based surveys (Laughlin et al. 2011; Enoch et al. 2012).
 449 Among *Kepler* giant planet candidates, inflation appears to occur only above an irradiance

450 of about $2 \times 10^8 \text{ ergs s}^{-1} \text{ cm}^{-2}$ (Demory & Seager 2011, hereafter D11).

451 Where information about stellar parameters is limited, spurious correlations can appear
 452 if two supposedly independent planetary parameters are related to the same, uncertain
 453 stellar parameter. In the absence of parallax or precise information on surface gravity, the
 454 radius of a star is constrained only by models of stellar atmospheres, stellar evolution, and
 455 galactic population. Uncertainty in stellar radius translates into corresponding uncertainties
 456 in both stellar luminosity and transiting planet radius. Because the radiation that a planet
 457 receives from a star is proportional to stellar luminosity, errors in irradiance and planet
 458 radius due to errors in stellar radius will be positively covariant. At least in principle, an
 459 apparent, positive trend between irradiation and planet radius could be created merely by
 460 errors in stellar radius.

461 We simulated the impact of this systematic with an analysis of KOIs similar to, but not
 462 identical to that of D11. We selected all KOIs with estimated radii of $8R_{\oplus} < R_p < 22R_{\oplus}$
 463 from B12, excluding those listed as false positives or “ambiguous” in Table 1 of D11. As
 464 in Section 3.1, we identified the best-fit Dartmouth model for each host star based on
 465 a χ^2 minimization of the difference with adjusted KIC values of T_e , $\log g$, and $[\text{Fe}/\text{H}]$,
 466 after applying corrections of -100 K to T_e and 0.17 dex to $[\text{Fe}/\text{H}]$ (Br11). We assumed
 467 standard deviations of 200 K, 0.36 dex, and 0.3 dex, respectively based on Br11 and 190
 468 stars where both KIC and spectroscopy-based parameters are available (B12). If no KIC
 469 value for $[\text{Fe}/\text{H}]$ was available we assumed solar metallicity. To estimate the maximum
 470 possible effect, no constraints other than the Dartmouth evolutionary tracks were used,
 471 i.e. we equally weighted masses, ages between 1-13 Gyr, and metallicities between -2.5 and
 472 +0.5 dex. Orbit-averaged stellar irradiation of the planet was calculated based on the model
 473 luminosity and mass, the orbital period, and assuming a circular orbit. (Non-circular orbits
 474 change the mean irradiance only slightly.) Planet radius was calculated from the transit

475 depth and stellar model radius and we did not account for limb darkening. The encircled
 476 points in Figure 6 indicate the best-fit planet radius vs. irradiance. Three KOIs (217.01,
 477 774.01, and 1547.01) have estimated irradiances $< 2 \times 10^8 \text{ ergs s}^{-1} \text{ cm}^{-2}$ and $R_p > 1.2R_J$,
 478 but only marginally so.

479 Fifteen KOIs have re-estimated radii $< 0.5R_J$ even though the values listed in B12
 480 exceed the criterion $> 0.714R_J$. Twelve of these have KIC impact parameters $b > 1$,
 481 suggesting problematic (or extreme grazing) transit solutions. Another (KOI 1419.01) has
 482 an implausible $b = 0.994$ which is inconsistent with its transit duration of $t = 1.36 \text{ h}$ and
 483 period $P = 1.36 \text{ d}$. KOI 377.02 (*Kepler* 9-b) has an erroneous transit depth reported in
 484 the MAST. The best-fit Dartmouth model assigns a somewhat smaller radius ($0.48R_\odot$) to
 485 the host star of KOI 1193.01 and thus makes the planet smaller as well. We excluded all
 486 planets with newly estimated radii $R_p < 8R_\oplus$ from our analysis.

487 We assessed the trends produced by correlated errors in planet radius and irradiation
 488 by considering all Dartmouth models that satisfy $\chi^2 < \chi_{min}^2 + 8.02$, where χ_{min}^2 is the
 489 minimum (best-fit) value, and 8.02 is the $\Delta\chi^2$ corresponding to a 95.4% (2σ) confidence
 490 interval for $\nu = 3$ degrees of freedom (stellar parameters). Because there are too many
 491 models to plot, we only show a random subsample of 200 such models for each KOI as
 492 the small points in Figure 6. These clearly show that correlated errors will tend to scatter
 493 points between the high irradiation/inflated and the low irradiation/uninflated regions of
 494 the diagram.

495 The paucity of KOIs with inflated radii ($R_p > 1.2R_J$) in the low irradiance region
 496 (upper right hand domain of Figure 6) supports the contention that the inflation of giant
 497 planets is related to stellar irradiation or planet equilibrium temperature. Furthermore,
 498 Kendall’s and Spearman’s rank correlation tests of all KOIs with $R_p > 0.714R_J$ yield
 499 τ values of 0.246 and 0.364, respectively, and corresponding p (significance) values of

500 4.6×10^{-5} and 3.1×10^{-5} . These low false-positive probabilities indicate a significant
 501 correlation between irradiation and plane radius. However, these statistics do not account
 502 for the systematic effect of correlated errors in radius and irradiation.

503 We simulated the effect of correlated errors by analyzing 10000 null realizations of
 504 the data where radii and orbital periods of KOIs were randomly shuffled among host stars
 505 and the transit depths were recomputed using Equation 1, thus destroying any intrinsic
 506 correlation between radius and irradiation. In computing each realization we include all
 507 KOIs with $R_p > 3R_\oplus$ to account for small planets that may appear larger, but in each
 508 Monte Carlo realization, as with the real sample, we limited the statistical analysis to
 509 $8-22R_\oplus$. New (“observed”) estimates of KIC stellar parameters were constructed from the
 510 “true” values by adding random, gaussian-distributed offsets with standard deviations of
 511 200 K for T_e , 0.36 dex for $\log g$, and 0.3 dex for [Fe/H]. Best-fit Dartmouth models were
 512 found for each parameter set, the planet radii and irradiation values were determined, and
 513 the correlation statistics were calculated. New p values for the fraction of KOIs in the
 514 low-irradiance/inflated-radius zone, and Kendall’s τ , and Spearman’s τ were computed as
 515 the fraction of MC realizations that are smaller (more significant) than the observed values.
 516 The distributions for the first two metrics are shown in Figs. 7 and 8 and the p values are
 517 1.4×10^{-3} and 6×10^{-4} , respectively. The result for the Spearman’s rank coefficient is
 518 similar, with $p = 6 \times 10^{-4}$.

519 3.6. Stellar metallicity and “shrunkn” Jupiters

520 Dodson-Robinson (2012, hereafter DR12) reported a weakly significant ($p = 0.02$
 521 or 2.3σ) trend of decreasing radius of *Kepler* (candidate) giant planet with increasing
 522 metallicity of the host star. She examined the ratio R_p/R_* of 218 KOIs from Borucki et al.
 523 (2011) with estimated radii of 5-20 R_\oplus and the correlation with estimated values of [Fe/H]

524 from the KIC. She interpreted the decline as evidence that giant planets around metal-rich
 525 stars have larger solid cores and, for the same total planet mass, smaller radii (Guillot
 526 2005).

527 Figure 9 is an updated version of Figure 1 in DR12 based on the more recent release of
 528 KOIs with revised radii (Batalha 2012). It includes 225 KOIs with $5R_{\oplus} < R_p < 20R_{\oplus}$ and
 529 host stars with KIC-determined metallicities. As in Figure 1 from DR12, a running median
 530 ($N = 21$) is plotted. The Kendall τ correlation coefficient is -0.032, indicating no significant
 531 correlation ($p = 0.48$). We were unable to reproduce the result of DR12 by simple cuts on
 532 this sample to approximate the earlier KOI sample, perhaps because many stellar radii (and
 533 hence planet radii) have been revised (Batalha 2012). We also emphasize that the values of
 534 $[\text{Fe}/\text{H}]$ in the KIC are no more accurate than ± 0.3 dex (Br11).

535 Irrespective of any physical phenomenon, one would expect to observe a decrease in
 536 R_p/R_* with increasing metallicity simply because metal-rich dwarfs tend to be larger than
 537 metal-poor dwarfs, and hence transit depths will be smaller (Equation 1). We modeled this
 538 effect with 10000 Monte Carlo realizations of the KOI catalog. There are two effects from
 539 increasing the radii of the host stars of a given planet population: one is that transit depths
 540 will become smaller and the planets will appear to be smaller. The other is that some
 541 planets may fall below the lower radius cutoff ($5R_{\oplus}$) and be excluded from the analysis.
 542 The reverse is true for lower metallicity; planets appear larger and a few planets may exceed
 543 the maximum cutoff ($20R_{\oplus}$). We therefore considered KOIs over a broader ($3\text{-}25R_{\oplus}$) range
 544 of radii, adopted this sample as representing the intrinsic (“true”) distribution of radii,
 545 estimated their apparent radii from the radius of the star and transit depth, and then
 546 applied the same radius criteria as DR12. We randomly shuffled the planet population
 547 among the host stars, thus destroying any intrinsic radius-metallicity correlation, computed
 548 the radii of the stars using the Dartmouth stellar evolution models, and re-calculated the

549 transit depths.

550 Each Monte Carlo host star was assigned the corrected T_e of the actual star it replaced.
 551 We assigned an *observed* metallicity based on the KIC value, a systematic correction
 552 Δ of 0.17 dex (Br11), a random normally-distributed error σ of 0.3 dex, and a prior
 553 distribution of *intrinsic* metallicities that is a gaussian with mean \bar{F} and standard deviation
 554 ϵ . This is equivalent to drawing metallicities from a single normal distribution with mean
 555 $(\epsilon^2(\bar{F} + \Delta) + \sigma^2\bar{F})/(\epsilon^2 + \sigma^2)$ and standard deviation $\epsilon^2\sigma^2/(\epsilon^2 + \sigma^2)$. The radius of each
 556 Monte Carlo star was taken to be the median of all model radii with $\log g > 4$ (presuming
 557 they are dwarf stars), $[\text{Fe}/\text{H}]$ within 0.15 dex of the Monte Carlo model, and T_e within
 558 100 K. We did not apply any age criterion other than 1-13 Gyr. We then calculated R_p/R_*
 559 using the shuffled planet radius and the median model radius stellar radius. For each Monte
 560 Carlo sample, we calculated Kendall's τ and false positive probability for a correlation
 561 between the *observed* metallicities and the artificial transit depths.

562 Median-filtered ($n = 21$) curves from these Monte Carlo realizations typically show a
 563 decline of R_p/R_* with increasing metallicity. Figure 10 shows the distribution of τ from
 564 10000 null realizations. The value of τ from the actual KOI sample is plotted as the dashed
 565 line. 61.6% of these null realizations produce a significant ($p < 0.01$) correlation and
 566 71.6% of values are below (and thus more significant than) the actual value of -0.032. For
 567 comparison the DR12 value is -0.17. Thus, negative correlations between metallicity and
 568 R_p/R_* are to be expected solely as a consequence of the metallicity-radius relation of stars,
 569 although these Monte Carlo simulations indicate that there is a $\sim 40\%$ chance that random
 570 errors in KIC $[\text{Fe}/\text{H}]$ values would prevent such a correlation from being detected.

4. Discussion

571

572 We have shown that selection effects for both transiting planets, and the target stars of
 573 transit surveys, combined with uncertainties in stellar radii, can bias the properties of host
 574 stars and their planets. These effects are in addition to those previously identified by Gaudi
 575 (2005), Gaudi et al. (2005), and Pont et al. (2006), which concern effects arising from the
 576 sensitivity of detection efficiency to planet radius and period. We have analyzed the effects
 577 of these systematics on the *Kepler* survey and its catalogs of target stars and candidate
 578 planets, using current models of stellar evolution and galactic stellar populations to infer
 579 the properties of *Kepler* stars. We did not apply constraints from the relation between
 580 stellar density, transit duration, and orbital period because the relation also depends on
 581 unknown orbital eccentricity and argument of periastron, and is not applicable to non-KOI
 582 stars.

583

584 We found that Eddington bias from the steep distribution of KOIs with radius results
 585 in an overestimation of the overall frequency of planets with $R_p > 2R_\oplus$ by about 15-20%
 586 of the actual value. We also find that Eddington bias acts to soften the “bump” in the
 587 distribution at Jupiter-size planets. This leads us to predict that the intrinsic peak at
 588 that radius is more pronounced. The effect on the distribution of smaller planets depends
 589 on whether the turnover in the radius distribution below $2R_\oplus$ is real, or the result of
 590 incompleteness. If the former, Eddington bias acts to flatten the apparent slope of the
 591 radius distribution, and in this case we predict that the actual slope is steeper than the
 592 $\alpha = 2.6$ power-law. Otherwise, the effect of Eddington bias on the power-law index is about
 0.1.

593

594 We made statistical estimates of Malmquist bias as a consequence of the magnitude
 595 limit of the target catalog. The estimated bias for two-thirds of KOI systems, including most
 KOIs smaller than Neptune, is $< 10\%$. However, we found that bias is more prevalent and

596 pronounced (up to a factor of two in radius) among larger candidate planets and their host
 597 stars, resulting from detection of these systems being governed by the apparent magnitude
 598 limit of the target catalog, rather than the SNR of transit detection. A Malmquist bias
 599 towards more luminous stars raises the possibility of inclusion of unidentified evolved stars
 600 within the *Kepler* target catalog (in addition to a number of deliberately selected and
 601 clearly identified giant stars). Nominally, stars with large radii were removed by a vetting
 602 process that used a criterion of *Kepler* detection of a $2R_{\oplus}$ planet (Batalha et al. 2010).
 603 However, KIC-derived stellar radii are based on estimates of $\log g$ and many of these
 604 are problematic. KIC photometry provides no information for the gravity of stars with
 605 $T_e > 5400\text{K}$ ($g - r < 0.65$), and subgiants would be assigned erroneously high $\log g$ (Br11).

606 There are bona fide subgiants hosting KOIs, e.g. the F5 subgiant HD 179070
 607 (Howell et al. 2012). Spectroscopy of stars hosting candidate giant planets has revealed
 608 other instances in which subgiants were misclassified as cooler, main sequence dwarfs in the
 609 KIC. Santerne et al. (2011) report a hot-Jupiter-hosting F-type subgiant ($M_* \approx 1.48M_{\odot}$,
 610 $R_* \approx 2.13R_{\odot}$). Based on spectra, they estimate $\log g = 4.1 \pm 0.2$, which is in contrast
 611 to its KIC value of 4.55. Likewise, the host of KOI-423b, assigned $\log g = 4.45$ in the
 612 KIC, is an F7IV subgiant with $\log g = 4.1$ (Bouchy et al. 2011). Three of five undiluted
 613 eclipsing binaries identified by Santerne et al. (2012) as false positives among *Kepler* giant
 614 planet candidates have masses larger than $1 M_{\odot}$, and one of these is definitely an evolved
 615 star. The mean difference between 190 pairs of KIC and spectroscopic values of $\log g$
 616 reported in Batalha (2012) is only 0.02 dex (standard deviation of 0.36 dex). Nevertheless,
 617 astroseismically-derived $\log g$ values average 0.05-0.17 dex lower than KIC values and
 618 astroseismically-determined radii are up to 50% larger (Verner et al. 2011; Bruntt et al.
 619 2012).

620 Among KOI-hosting stars whose radius has been underestimated, small planets may

621 actually be larger, even Jupiter-size planets. In turn, giant “planets” may turn out to be
 622 diluted or undiluted stellar companions, a significant source of astrophysical false positives
 623 in transit surveys (Charbonneau et al. 2004; Almenara et al. 2009). Based on a preliminary
 624 Doppler survey, Santerne et al. (2012) estimated that about 40% of candidate giant planets
 625 are false positives and about one quarter of those are undiluted eclipsing binaries. This
 626 also means that estimates of the occurrence of Jupiters on close-in orbits (Howard et al.
 627 2012) must be revised downwards. Wright et al. (2012) report that the occurrence of “hot
 628 Jupiters” ($P < 10$ d) in the *Kepler* catalog is only half that seen in Doppler surveys, and
 629 adjustment for a high false-positive rate would worsen this discrepancy.

630 One explanation for the discrepancy between the *Kepler* and Doppler surveys might
 631 be the presence of misidentified subgiant stars in the *Kepler* target catalog. The intrinsic
 632 distribution of planets may be different around evolved stars compared to main sequence
 633 stars. Planets have been discovered around subgiant stars (Butler et al. 2006), but giant
 634 planets appear to be rare with 0.6 AU ($P < 120$ d) of clump GK giants (Sato et al. 2008,
 635 2010; Johnson et al. 2011) - CoRoT-21b may be an exception (Patzold et al. 2011). The
 636 timescale of the decay of a planet’s orbit due to dissipation of tides in a star’s convective
 637 envelope scales as $R_*^{-8} M_{env}$, where M_{env} is the mass of the envelope. Hot Jupiters are likely
 638 to be destroyed by infall and disruption inside the Roche lobe as a star evolves off the main
 639 sequence, expands, and its convective envelopes thicken (Kunitomo et al. 2011). Thus,
 640 one explanation for the comparative paucity of hot Jupiters in the KOI catalog is that,
 641 because of Malmquist bias, many *Kepler* targets are older stars or subgiants for which hot
 642 Jupiters cannot be detected, have been miscategorized as Neptunes, or have been destroyed
 643 by orbital decay. A comparison between the distributions of $\log g$ predicted by TRILEGAL
 644 and that of the KIC suggest no large ($>10\%$) population of unidentified subgiants, however
 645 spectroscopy of candidate subgiants is needed to actually test this conjecture.

646 We have shown that, because metal-poor stars tend to have smaller radii than their
647 metal-rich counterparts, stars with transiting planets will be biased towards metal-poor
648 members, independent of any correlation between planets and metallicity. However, we
649 estimate that this metallicity bias is only about -0.02 dex and can be neglected. Thus a
650 comparison between the mean metallicity of stars with transiting planets and that of the
651 overall target population is appropriate. The mean metallicity of M dwarfs with KOIs,
652 -0.09 (Muirhead et al. 2012), and solar-type stars with small planets, -0.01 (Buchhave et al.
653 2012), appears similar to that of the solar neighborhood: Schlaufman & Laughlin (2010)
654 report a mean metallicity of -0.14 ± 0.06 for a volume-limited local sample of M dwarfs
655 using a photometric calibration, and Casagrande et al. (2011) report a median metallicity of
656 -0.06 for all stars in the solar neighborhood. Whether the overall *Kepler* target population
657 has a similar metallicity distribution is not yet known and additional observations are
658 required. From our calculations we conclude that such a comparison would not suffer from
659 significant metallicity bias, but must take into account a dilution factor because stars
660 without transiting planets are not necessarily stars without planets. This dilution factor is
661 large for a high planet occurrence (Mann et al. 2012).

662 We have shown how uncertainties in stellar radius or distance produce correlated errors
663 in a planet’s radius and the radiation received from the host star. This effect can produce
664 an artificial correlation in populations of planets where none exists. Recently, such a
665 correlation has been found in both ground-based transit surveys and the *Kepler* catalog, and
666 highlighted as a test of mechanisms to explain the “inflation” of giant planets on close-in
667 orbits. We quantified the systematic effect of correlated errors in stellar radius in the case
668 of the *Kepler* KOIs and show that, despite this systematic, the result of D11, i.e. that
669 inflated planets are absent at low irradiance, is still significant. To maximize any systematic
670 effect, we used a very broad range of metallicities (-2.5 to +0.5) and no constraint on
671 stellar distance (e.g., from a model of galactic structure), thus further strengthening our

672 conclusion.

673 Finally, we have shown how searches for trends of transiting planet radius with stellar
 674 properties may engender systematic errors unless the effect of those properties on apparent
 675 stellar radius - and hence planet radius - is taken into account. We examined the tentative
 676 (2.3σ) claim of DR12 that giant planets around metal-rich stars tend to have smaller
 677 transit depths, because they are smaller and perhaps have larger rocky cores. Performing a
 678 similar analysis on the most recent KOI catalog, we were unable to reproduce that trend.
 679 Moreover, we performed simulations that show that the trend observed by DR12 could be
 680 easily explained by the dependence of stellar radius on metallicity.

681 Two limitations of our analysis are that (i) we have assumed gaussian-distributed
 682 errors in the corrected KIC parameters T_e , $\log g$, and $[\text{Fe}/\text{H}]$, and (ii) that the construction of
 683 Bayesian priors on mass, age, and metallicity treat them as independent variables. Neither
 684 of these is absolutely correct; the first assumption probably produces an underestimate of
 685 the uncertainty in stellar radius while the second assumption produces an overestimate of
 686 the uncertainty. Of course, any inadequacies in the Dartmouth stellar evolution models
 687 themselves are not accounted for.

688 There are other systematics effects which may be present in transit surveys. Two-thirds
 689 of solar-type (F6-K3) stars are found in multiple systems (Raghavan et al. 2010). At
 690 the typical distance of *Kepler* KOIs with solar-type hosts (950 pc), one 4 arc-second
 691 pix subtends about 3800 AU, sufficient to include nearly all companions to primaries
 692 (Lépine et al. 2007; Raghavan et al. 2010). The presence of an unresolved companion,
 693 or any background star, will dilute the transit signal. Transits otherwise just above the
 694 detection threshold might be rendered invisible. As a consequence, members of multiple
 695 systems may be underrepresented among stars with transiting planets. For equal-mass
 696 binaries (twins) where the transit signal is lower by a factor of 2, the fractional noise will

697 decrease by $\sqrt{2}$ (due to the doubling of the signal compared to a comparable single star)
 698 and thus the radius of the smallest detectable planet will increase by a factor of $2^{1/4}$, or
 699 about 1.2. For a power-law size distribution (Equation 3), the number of detectable planets
 700 *per star* will decrease by a factor of $2^{-\alpha/4}$, or 0.64 for $\alpha = 2.6$. However, nearly-equal mass
 701 binaries represent only 12% of all binaries (Raghavan et al. 2010) and systems with mass
 702 ratios < 1 and luminosity ratios $\ll 1$, where the dilution will be much smaller, are the
 703 norm. Star counts reach $\sim 1000 \text{ mag}^{-1} \text{ deg}^{-2}$ at $K_p = 16$, and so there is only a few %
 704 chance of significant dilution by an unrelated star. To the extent that stellar variability
 705 inhibits transit detection, younger, and more active stars will be also underrepresented
 706 among KOIs.

707 The best defense against the systematic errors we have described is better
 708 characterization of the target stars of transit surveys, especially those hosting planets.
 709 This will reduce, but not entirely eliminate, these biases. Spectroscopic characterization
 710 and refinement of the properties of a fully representative sample of *Kepler* target stars,
 711 not just the KOI hosts, is vital to robust statistical analyses of the properties of transiting
 712 planets and their parent stars stars, and such programs are underway (Mann et al. 2012;
 713 Buchhave et al. 2012). Spectra of modest resolution ($R < 1000$) (Malyuto et al. 2001) or
 714 SNR (~ 10) (Katz et al. 1998) (but not both) can provide substantial improvements over
 715 photometry alone. The *Gaia* (originally Global Astrometric Interferometer for Astrophysics)
 716 mission, scheduled for launch in August 2013, will obtain parallaxes of stars as faint as
 717 16th magnitude with a standard error of $\leq 40 \mu\text{as}$ (de Bruijne 2012). This will allow the
 718 luminosity of a solar-type star to be determined with an error about 15% and its radius with
 719 an error of about 8%. The distance to brighter stars will be measured with even greater
 720 precision. *Gaia* will also obtain moderate-resolution spectra in a narrow region centered
 721 on the Ca II triplet region which can be used to classify stars (Kordopatis et al. 2011) and
 722 measure their radial velocities to a precision of a few km sec^{-1} . Radial velocities, combined

723 with parallaxes, yield space motions and membership in distinct stellar populations (e.g.
724 thin disk, halo). *Gaia* data will also benefit future transit surveys that will cover all of or a
725 large part of the sky (Deming et al. 2009).

726 This research was supported by NSF grants AST-09-08406 and NASA grants
727 NNX10AI90G and NNX11AC33G to EG. The *Kepler* mission is funded by the NASA
728 Science Mission Directorate, and data were obtained from the Mukulski Archive at the
729 Space Telescope Science Institute, funded by NASA grant NNX09AF08G.

REFERENCES

730

731 Agol, E., Steffen, J. H., Sari, R., & Clarkson, W. 2005, *Mon. Not. Royal Astron. Soc.*, 359,
732 567

733 Almenara, J. M., et al. 2009, *Astron. Astrophys.*, 506, 337

734 Baraffe, I., Chabrier, G., Barman, T. S., Allard, F., & Hauschildt, P. H. 2003, *Astron.*
735 *Astrophys.*, 712, 701

736 Batalha, N. M. 2012, arXiv:1202.5852

737 Batalha, N. M., et al. 2010, *Astrophys. J.*, 713, L109

738 Batygin, K., & Stevenson, D. J. 2010, *Astrophys. J.*, 714, L238

739 Bean, J. L., Seifahrt, A., Hartman, H., Nilsson, H., Wiedemann, G., Reiners, A., Dreizler,
740 S., & Henry, T. J. 2010, *Astrophys. J.*, 713, 410

741 Bodenheimer, P., Lin, D. N. C., & Mardling, R. A. 2001, *Astrophys. J.*, 548, 466

742 Borucki, W. J., et al. 2011, *Astrophys. J.*, 736, article id. 19

743 Bouchy, F., et al. 2011, *Astron. Astrophys.*, 533, 83

744 Boyajian, T. S., et al. 2012, *Astrophys. J.*, 757, 112

745 Brown, T. M., Latham, D. W. D., Everett, M. E. M., & Esquerdo, G. G. a. 2011, *Astron.*
746 *J.*, 142, 112

747 Bruntt, H., et al. 2012, *Mon. Not. Royal Astron. Soc.*, 423, 122

748 Buchhave, L. a., et al. 2012, *Nature*, 486, 375

- 749 Burrows, A., Guillot, T., Hubbard, W., Marley, M. S., Saumon, D., Lunine, J. I., &
750 Sudarsky, D. 2000, *Astrophys. J.*, 534, L97
- 751 Butler, R. P., Johnson, J. A., Marcy, G. W., Wright, J. T., Vogt, S. S., & Fischer, D. A.
752 2006, *Publ. Astron. Soc. Pac.*, 118, 1685
- 753 Casagrande, L., Schoenrich, R., Asplund, M., Cassisi, S., Ramirez, I., Melendez, J., Bensby,
754 T., & Feltzing, S. 2011, *Astron. Astrophys.*, 530, A138
- 755 Charbonneau, D., & Brown, T. 2000, *Astrophys. J.*, 529, L45
- 756 Charbonneau, D., Brown, T. M., Dunham, E. W., Latham, D. W., Looper, D. L., &
757 Mandushev, G. 2004, in *The Search for Other Worlds: 14th Astrophysics Conference*,
758 Vol. 713 (Melville, NY: AIP), 151–160
- 759 Charbonneau, D., Brown, T. M., Noyes, R. W., & Gilliland, R. L. 2002, *Astrophys. J.*, 568,
760 374
- 761 Charbonneau, D., & Deming, D. 2007, arXiv:0706.1047
- 762 Charbonneau, D., et al. 2005, *Astrophys. J.*, 626, 523
- 763 Cox, A. N. 2000, *Allen’s Astrophysical Quantities* (New York: AIP Press, Springer)
- 764 Cumming, A., Butler, R., Marcy, G., & Vogt, S. 2008, *Publ. Astron. Soc. Pac.*, 120, 531
- 765 de Bruijne, J. H. J. 2012, *Astrophys. Space Sci.*, online first
- 766 Deming, D., et al. 2009, *Publ. Astron. Soc. Pac.*, 121, 952
- 767 Demory, B.-O., & Seager, S. 2011, *Astrophys. J. Supp. Ser.*, 197, 12
- 768 Désert, J.-M., Kempton, E. M.-R., Berta, Z. K., Charbonneau, D., Irwin, J., Fortney, J.,
769 Burke, C. J., & Nutzman, P. 2011, *Astrophys. J.*, 731, L40

- 770 Dodson-Robinson, S. E. 2012, *Astrophys. J.*, 752, 72
- 771 Dotter, A., Chaboyer, B., Jevremović, D., Kostov, V., Baron, E., & Ferguson, J. W. 2008,
772 *Astrophys. J.*, 178, 89
- 773 Eddington, A. S. 1913, *Mon. Not. Royal Astron. Soc.*, 73, 359
- 774 Enoch, B., Collier-Cameron, A., & Horne, K. 2012, *Astron. Astrophys.*, 540, 99
- 775 Fischer, D. A., & Valenti, J. 2005, *Astrophys. J.*, 622, 1102
- 776 Ford, E. B., et al. 2011, *Astrophys. J. Supp. Ser.*, 197, 2
- 777 Fortney, J. J., Baraffe, I., & Militzer, B. 2010, in *Exoplanets* (University of Arizona Press),
778 397
- 779 Fressin, F., Guillot, T., & Nesta, L. 2009, *Astron. Astrophys.*, 504, 605
- 780 Gaidos, E., Fischer, D. A., Mann, A. W., & Lépine, S. 2012, *Astrophys. J.*, 746, 36
- 781 Gaidos, E., Haghighipour, N., Agol, E., Latham, D., Raymond, S. N., & Rayner, J. 2007,
782 *Science*, 318, 210
- 783 Gaudi, B. S. 2005, *Astrophys. J.*, 628, L73
- 784 Gaudi, B. S., Seager, S., & MallenOrnelas, G. 2005, *Astrophys. J.*, 623, 472
- 785 Girardi, L., Groenewegen, M., Hatziminaoglou, E., & Da Costa, L. 2005, *Astron. Astrophys.*,
786 436, 895
- 787 Gonzalez, G. 1998, *Astron. Astrophys.*, 238, 221
- 788 Grasset, O., Schneider, J., & Sotin, C. 2009, *Astrophys. J.*, 693, 722
- 789 Guillot, T. 2005, *Annu. Rev. Earth Planet. Sci.*, 33, 493

- 790 Guillot, T., Burrows, A., Hubbard, W., Lunine, J. I., & Saumon, D. 1996, *Astrophys. J.*,
791 459, L35
- 792 Henry, G. W., Marcy, G. W., Butler, R. P., & Vogt, S. S. 2000, *Astrophysical Journal*, 529,
793 L41
- 794 Howard, A. W., et al. 2010, *Science*, 330, 653
- 795 —. 2012, *Astrophys. J. Supp. Ser.*, 201, 15
- 796 Howell, S. B., et al. 2012, *Astrophys. J.*, 746, 123
- 797 Huber, D., et al. 2010, *Astrophys. J.*, 723, 1607
- 798 Johnson, J., Clanton, C., & Howard, A. 2011, *Astrophys. J.*, 197, 26
- 799 Johnson, J. J., Aller, K. K., Howard, A. A., & Crepp, J. 2010, *Publ. Astron. Soc. Pac.*, 122,
800 233
- 801 Katz, D., Soubiran, C., Cayrel, R., Adda, M., & Cautain, R. 1998, *Astron. Astrophys.*, 160,
802 151
- 803 Knutson, H. A., Charbonneau, D., Allen, L. E., Burrows, A., & Megeath, S. T. 2008,
804 *Astrophys. J.*, 673, 526
- 805 Konacki, M., Torres, G., Jha, S., & Sasselov, D. D. 2003, *Nature*, 421, 507
- 806 Kordopatis, G., Recio-Blanco, A., de Laverny, P., Bijaoui, A., Hill, V., Gilmore, G., Wyse,
807 R. F. G., & Ordenovic, C. 2011, *Astron. Astrophys.*, 535, A106
- 808 Kroupa, P. 2002, in *Modes of Star Formation and the Origin of Field Populations*. ASP
809 Conference Series Vol. 285, ed. E. K. Grebel & W. Brandner (ASP)
- 810 Kunitomo, M., Ikoma, M., Sato, B., Katsuta, Y., & Ida, S. 2011, *Astrophys. J.*, 737, 66

- 811 Laughlin, G., Crismani, M., & Adams, F. C. 2011, *Astrophys. J.*, 729, L7
- 812 Lepine, S., Hilton, E. J., Mann, A. W., Wilde, M., Rojas-Ayala, B., Cruz, K. L., & Gaidos,
813 E. 2012, arXiv1206.5991L
- 814 Lépine, S., Rich, R. M., & Shara, M. M. 2007, *Astrophys. J.*, 669, 1235
- 815 Lissauer, J. J., et al. 2012, *Astrophys. J.*, 750, 112
- 816 Liu, W. M., & Chaboyer, B. 2000, *Astrophys. J.*, 544, 818
- 817 Malmquist, K. G. 1922, *Lund Medd. Ser. I*
- 818 Malyuto, V., Lazauskaite, R., & Shvelidze, T. 2001, *New Astron.*, 6, 381
- 819 Mann, A. W., Gaidos, E., Lepine, S., & Hilton, E. J. 2012, *Astrophys. J.*, 753, 90
- 820 Mayor, M., et al. 2009, *Astron. Astrophys.*, 493, 527
- 821 —. 2011, *Astron. Astrophys.*, 507, 487
- 822 Mizuno, H. 1980, *Prog. Theor. Phys.*, 64, 544
- 823 Morton, T. T. D., & Johnson, J. A. J. 2011, *Astrophys. J.*, 738, 170
- 824 Muirhead, P., Hamren, K., Schlawin, E., Rojas-Ayala, B., Covey, K. R., & Lloyd, J. P.
825 2012, *Astrophys. J.*, 750, L37
- 826 Oswalt, T. D., Smith, J. A., Wood, M. A., & Hintzen, P. 1996, *Nature*, 382, 692
- 827 Patzold, M., Endl, M., Czismadia, S., Gandolfi, D., Jorda, L., Grziwa, S., Carone, L., &
828 Pasternacki, T. 2011, in EPSC-DPS Joint Meeting, 1192
- 829 Pinsonneault, M., An, D., Molenda-akowicz, J., Chaplan, W. J., Metcalfe, T. S., & Bruntt,
830 H. 2012, *Astrophys. J. Supp. Ser.*, 199, 30

- 831 Pont, F., Zucker, S., & Queloz, D. 2006, *Mon. Not. Royal Astron. Soc.*, 373, 231
- 832 Raghavan, D., et al. 2010, *Astrophys. J. Supp. Ser.*, 190, 1
- 833 Rogers, L., Bodenheimer, P., Lissauer, J., & Seager, S. 2011, *Astrophys. J.*, 738, 59
- 834 Rowe, J. F., et al. 2008, *Astrophys. J.*, 689, 1345
- 835 Ruchti, G. R., et al. 2011, *Astrophys. J.*, 737, 9
- 836 Santerne, A., Bouchy, F., Deleuil, M., Moutou, C., Eggenberger, A., Ehrenreich, D., Gry,
837 C., & Udry, S. 2011, *Astron. Astrophys.*, 528, A63
- 838 Santerne, A., Moutou, C., Bouchy, F., Bonomo, A. S., Deleuil, M., & Santos, N. C. 2012,
839 *Astron. Astrophys.*, 545, 76
- 840 Santos, N. C., Israelian, G., & Mayor, M. 2004, *Astronomy and Astrophysics*, 415, 1153
- 841 Sato, B., Toyota, E., Omiya, M., & Izumiura, H. 2008, *Publ. Astron. Soc. Japan*, 60, 1317
- 842 Sato, B., et al. 2010, *Publ. Astron. Soc. Japan*, 62, 1063
- 843 Schlaufman, K., & Laughlin, G. 2011, *Astrophys. J.*, 738, 177
- 844 Schlaufman, K. C., & Laughlin, G. 2010, *Astron. Astrophys.*, 519, A105
- 845 Schlegel, D., Finkbeiner, D., & Davis, M. 1998, *The Astrophysical Journal*, 500, 535
- 846 Schneider, J., Dedieu, C., Sidaner, P. L., Savalle, R., & Zolotukhin, I. 2011, *Astronomy and*
847 *Astrophysics*, 532, A79
- 848 Seager, S., Kuchner, M. J., Hier-Majumder, C., Militzer, B., & HierMajumder, C. a. 2007,
849 *Astrophys. J.*, 669, 1279
- 850 Showman, A. 2002, *Astron. Astrophys.*, 385, 166

- 851 Sousa, S. G., et al. 2008, *Astron. Astrophys.*, 381, 373
- 852 Tarter, J. C., et al. 2007, *Astrobiology*, 7, 30
- 853 Valencia, D., Sasselov, D. D., & O’Connell, R. J. 2007, *Astrophys. J.*, 665, 1413
- 854 Vanhollebeke, E., Groenewegen, M. a. T., & Girardi, L. 2009, *Astron. Astrophys.*, 498, 95
- 855 Verner, G. a., et al. 2011, *The Astrophysical Journal*, 738, L28
- 856 Wolfgang, A., & Laughlin, G. 2012, *Astrophys. J.*, 750, 148
- 857 Woolf, V. M., & West, A. A. 2012, *Mon. Not. Royal Astron. Soc.*, 422, 1489
- 858 Wright, J., Marcy, G., Howard, A., Johnson, J. A., Morton, T., & Fischer, D. A. 2012,
859 *Astrophys. J.*, 753, 160
- 860 Zielinski, P., Niedzielski, A., Wolszczan, A., Adamow, M., & Nowak, G. 2012,
861 [arXiv:1206.6276](https://arxiv.org/abs/1206.6276)

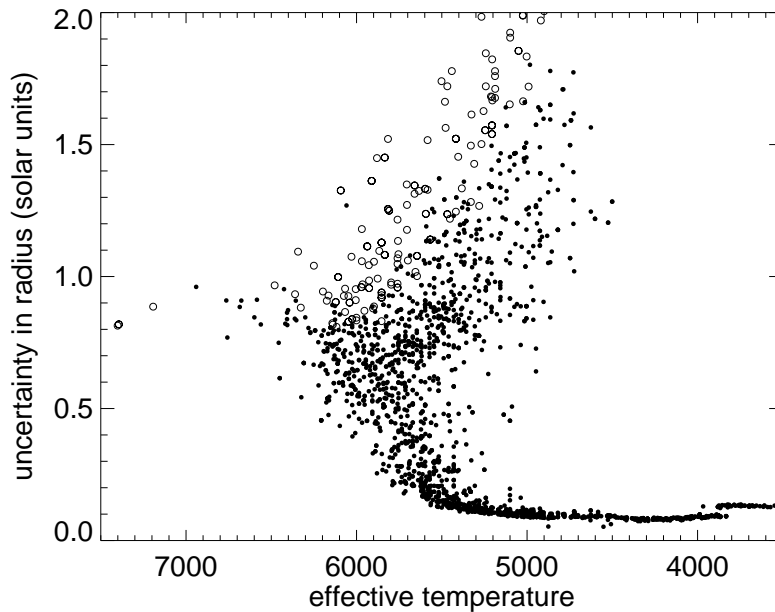


Fig. 1.— Uncertainty in radius of stars hosting KOIs, defined as one half of the range encompassing 68% of the probability distribution of radii. A few stars with the largest uncertainty are off-scale. As defined, the uncertainty can exceed the mean or most likely value and does in some cases. The adjusted KIC effective temperature is plotted on the abscissa. Solid points have KIC $\log g > 4$ (“dwarfs”), while open points have $\log g < 4$ (“giants”). While K-type dwarfs have uncertainties of as little as $\sim 15\%$, the radius of F- and many G-type stars is uncertain by $\geq 100\%$ because of the proximity of the giant and dwarf branches. The discontinuity at $T_e \sim 3900$ K is an artifact of the grid of models and the sensitivity to very large M giants.

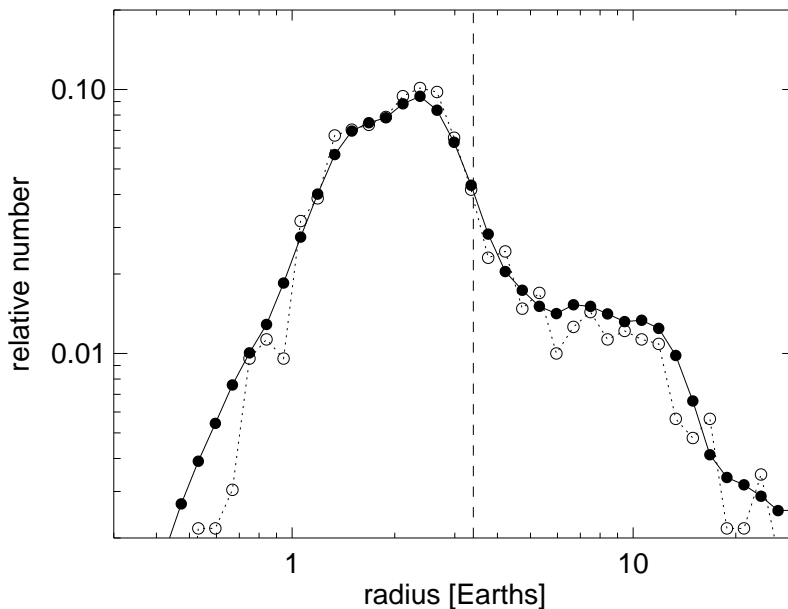


Fig. 2.— Observed (uncorrected) distribution of KOI radii (open points and dashed line), and a distribution simulating the effects of Eddington bias (filled points and solid line). The latter is constructed by adjusting the ratio of each planet candidate by the ratio of the most likely stellar radius to every possible radius among stellar models, weighted by a likelihood factor (Equation 19). The two normalized distributions are equal at $R_p = 3.4R_\oplus$. The biased distribution has a shallower slope at small radii, a less pronounced bump at Jupiter-size, and a higher occurrence of planets larger than the completeness limit.

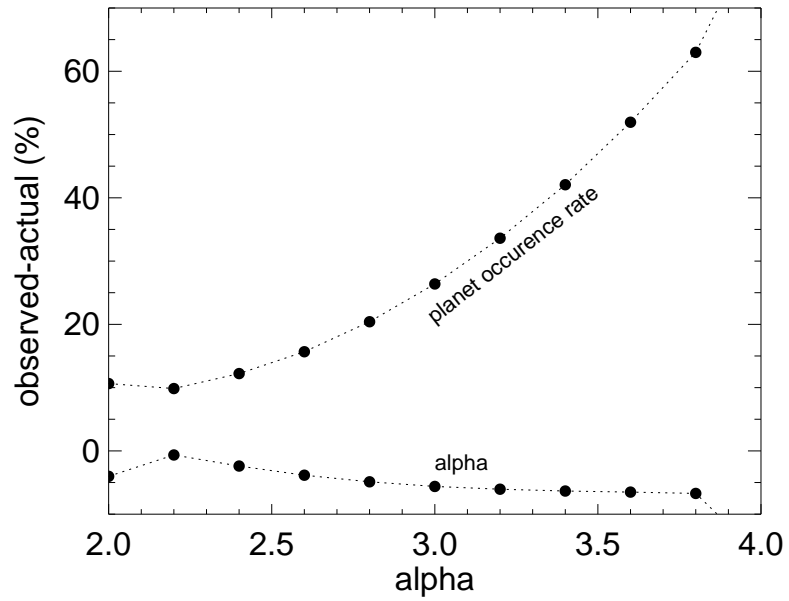


Fig. 3.— Predicted biases in planet occurrence and power-law slope α due to Eddington bias for artificial planets with a power-law radius distribution placed around *Kepler* KOI-hosting stars. Howard et al. (2012) report that $\alpha \approx 2.6$ for planets with periods $P < 50$ d. The slope of the scale-free power law distribution is only slightly affected by Eddington bias, but the apparent occurrence is biased upwards because more numerous smaller planets appear as larger planets due to errors in stellar radius.

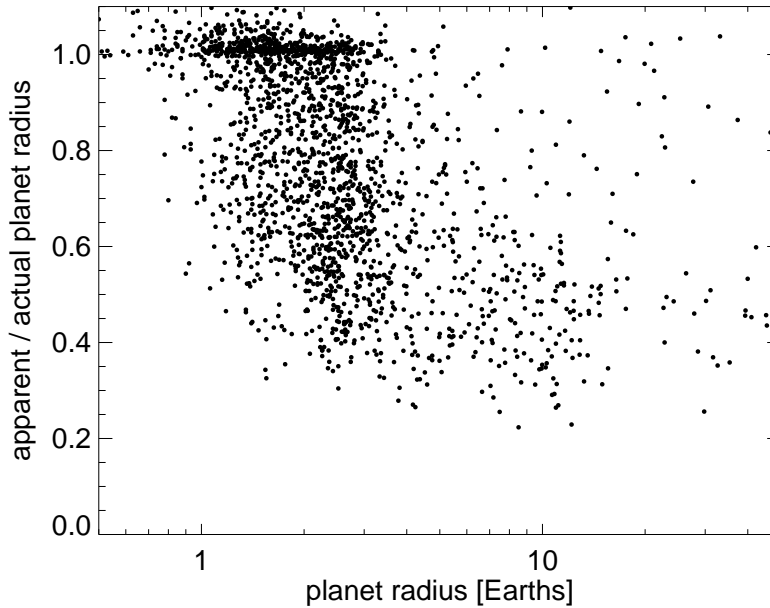


Fig. 4.— Effect of Malmquist bias on the radii of stars and their planets. The ratio of the apparent or “naive” radius to the actual or “bias-informed” radius of 2061 KOIs is plotted vs. the nominal planet radius from the catalog of Batalha (2012). (239 others are around stars with incomplete parameters from the Kepler Input Catalog). The “naive” radius is the mean radius of possible stellar models weighted according to their consistency with KIC parameters and priors of mass, age, and metallicity. The “bias-informed” radius is the mean calculated using the scaling laws for Malmquist bias derived in Section 2.2. 1254 KOIs, and the vast majority of planet candidates smaller than Neptune, have predicted bias $<10\%$, but many giant “planets” may have radii twice the nominal value and some may be astrophysical false positives, i.e. eclipsing stars.

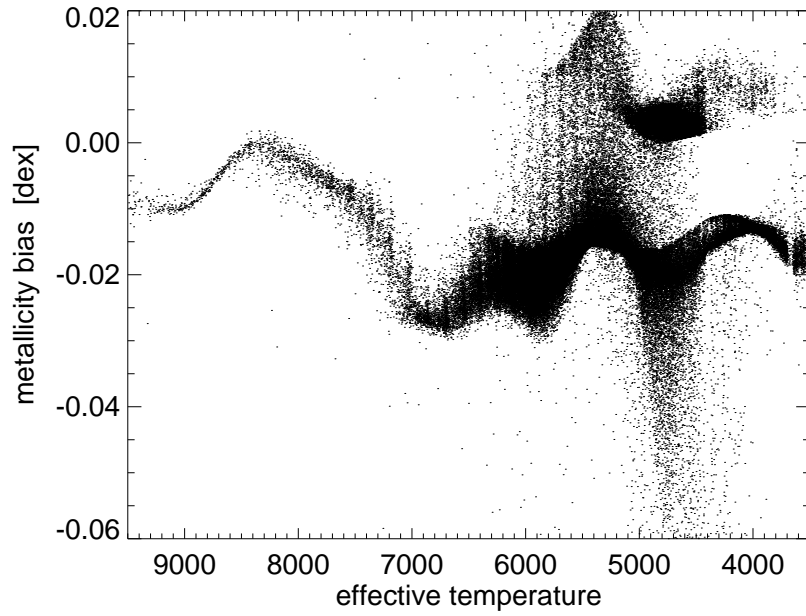


Fig. 5.— Predicted bias in metallicity in transiting planet-selected stars as a consequence of the relationships between transit depth, stellar radius, and stellar metallicity. The bias was calculated for all Quarter 6 *Kepler* target stars (regardless of whether or not they host KOIs) using Eqns. 2 and 11 and the methods described in Section 3.1. The upper locus of positive values are evolved stars, for which radius *decreases* with increasing metallicity.

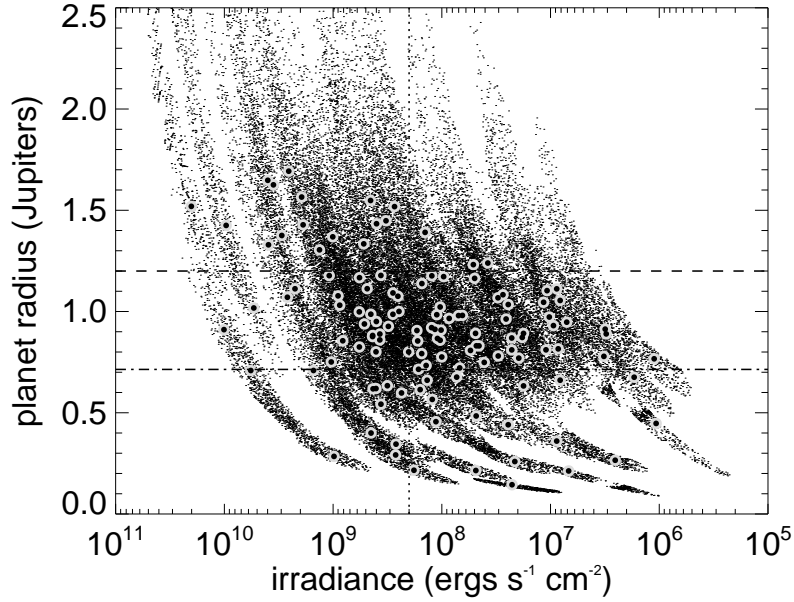


Fig. 6.— Radius vs. stellar irradiance of candidate giant planets ($8R_{\oplus} < R_P < 22R_{\oplus}$) in the latest KOI release. These exclude the KOIs listed as false positives or “ambiguous” in the Table 1 of Demory & Seager (2011). Each large point represents values based on the stellar radius and luminosity of the Dartmouth stellar model that best reproduces the stellar parameters from the KIC. The dots represent 200 models chosen randomly from among all Dartmouth stellar models that cannot be ruled out at 95.4% (2σ) confidence. The vertical dotted line demarks the suggested boundary between high and low stellar irradiation regimes. Objects above the horizontal dashed line ($1.2R_J$) are considered “inflated”. Objects below the dot-dashed line ($8R_{\oplus}$) are smaller than reported in the KOI catalog and may have problematic *Kepler* lightcurve analyses. These were not included in the statistical analysis.

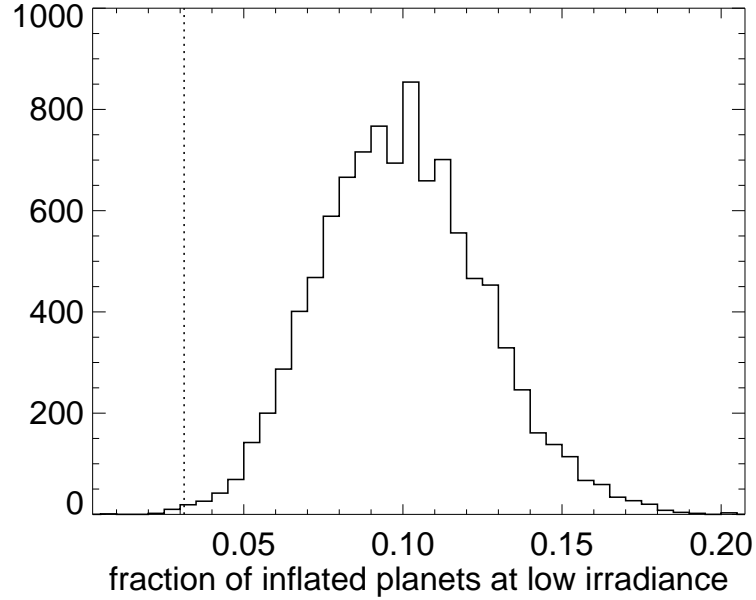


Fig. 7.— Fraction of “inflated” ($R_p > 1.2R_J$) candidate planets in the low irradiance ($<2 \times 10^8$ ergs sec $^{-1}$ cm $^{-2}$) regime in 1000 Monte Carlo simulations of the KOI data set where planets were randomly shuffled among stars and stellar parameters were resampled according to standard errors in the KIC values. All KOIs with $R_p > 3R_\oplus$ were used to generate the artificial planet populations, but only planets with $R_p > 8R_\oplus$ were used in the analysis. The vertical dashed line marks the actual number (3). The p value based on this distribution is 1.4×10^{-3} .

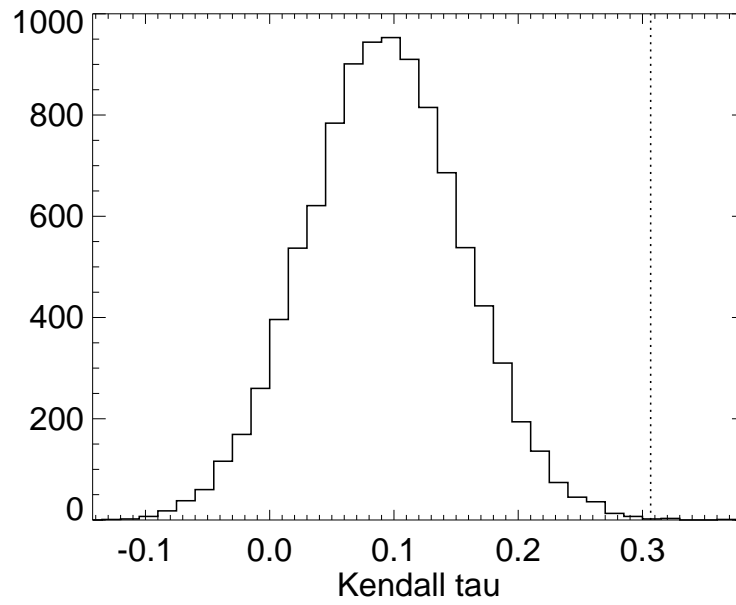


Fig. 8.— Distribution of 1000 Kendall τ values for the correlation between planet radius and stellar irradiance using the same Monte Carlo realizations of the giant planet KOIs as in Figure 7. The vertical dashed line marks the actual value ($\tau = 0.31$), corresponding to a significance (p value) of 6×10^{-4} .

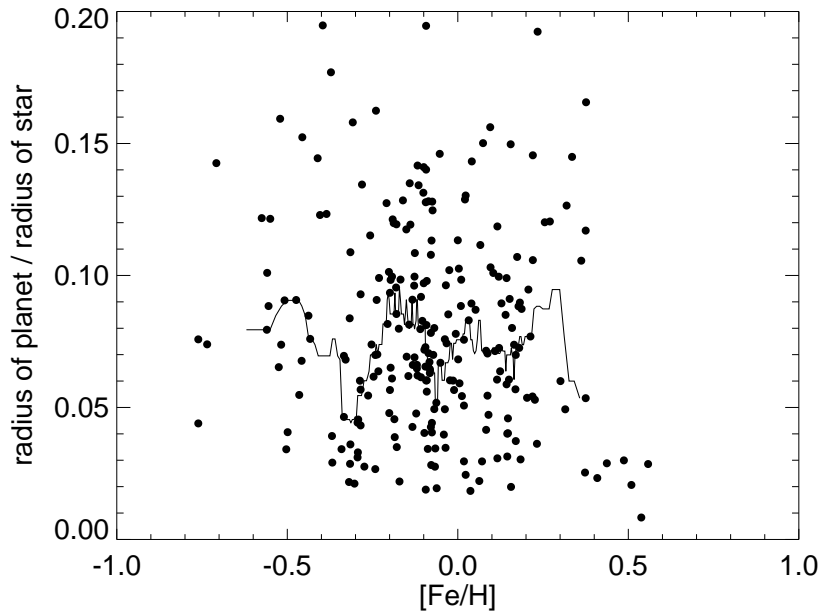


Fig. 9.— Ratio of planet radius to star radius of 225 *Kepler* candidate planets with estimated radii between 5 and 20 R_p vs. metallicity estimates from the *Kepler* Input Catalog metallicities, uncertain by 0.3 dex (Br11). The curve is a running median ($n=21$). No trend with metallicity is apparent.

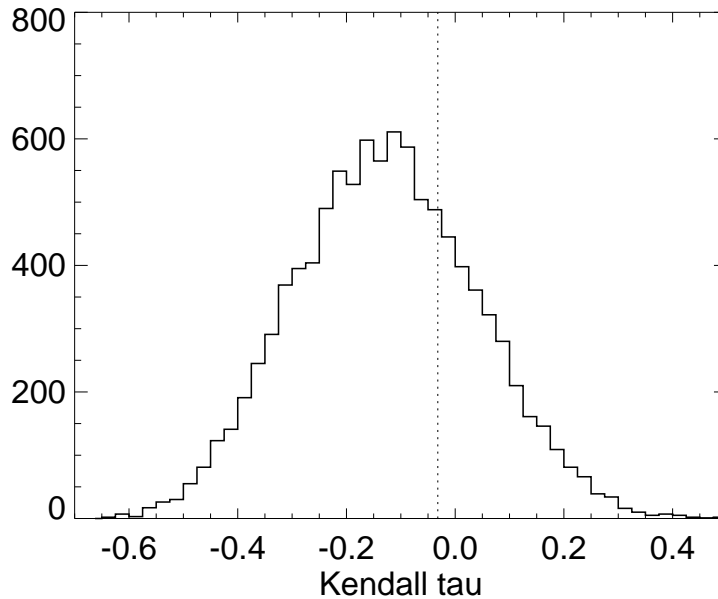


Fig. 10.— Distribution of Kendall τ values among 10000 Monte Carlo simulations of the KOI data set shown in Figure 9. Host star metallicities and KOI radii are scrambled, removing any intrinsic correlation between metallicity and planet radii. The only correlation here is due to the increasing radius of stars with metallicity. The dotted line is the value from the actual data. 3σ significance correspond to $\tau \approx -0.13$. Therefore, there is no significant correlation in the real data, and, because of the dependence of stellar radius on metallicity, a null sample would contain a significant ($p < 0.01$) correlation about 60% of the time.

Table 1: Parameter values for TRILEGAL 1.5

Parameter	Value
Dust:	
Extinction at ∞	0.0378
Scale height	110 pc
Scale length	100 kpc
Position of Sun:	
Galactocentric radius	8700 pc
Height above disk	24.2 pc
Thin disk:	
Zero-age scale height	95 pc
Radial length scale	2.8 kpc
Local surface density	$59 M_{\odot} \text{ pc}^{-2}$
Star formation rate	2-step
Thick disk:	
Scale height	800 pc
Radial length scale	2.8 kpc
Local density	$1.5 \times 10^{-3} M_{\odot} \text{ pc}^{-2}$
Star formation rate	11-12 Gyr constant
Halo:	
Shape	$r^{1/4}$ spheroid
Scale length	2.8 kpc
Oblateness	0.65
Local density	$1.5 \times 10^{-4} M_{\odot} \text{ pc}^{-2}$
Star formation rate	12-13 Gyr